UNIVERSITÀ POLITECNICA DELLE MARCHE

FACOLTÀ DI INGEGNERIA

Master's Degree in Biomedical Engineering

ELECTROMAGNETIC EXPOSURE DUE TO WEARABLE DEVICES: ANALYSIS OF THE SMARTWATCH - HUMAN TISSUE INTERACTION

Advisor:

Prof. FRANCO MOGLIE

Co-Advisor:

Prof. VALTER MARIANI PRIMIANI

Candidate:

TITO SGRO

ACADEMIC YEAR: 2019/2020

INDEX

Abstract

Wearable devices are used routinely today by the majority of people, since they have proved to be of immense benefit. In particular, smartwatches are regarded as the first commercialized wearable devices for consumers and represent a significant development in the domain of wearable technology. The fast expansion of the use of wearable devices and the extraordinarily growth IoT wearables market have had the unintended consequence of creating a knowledge gap in the study of interactions between the device and human tissues.

The majority of studies on smartwatches have been focused on the usability, the perceived value, and the fashion perception of them. Since these devices are in close contact with the human body and continuously emit a small amount of EMF radiation, the question is if they could be harmful to the user's health. Thus, the purpose of this study is the electromagnetic characterization of the wrist, useful for the determination, through FDTD simulations, of the effects of the electromagnetic fields generated by Bluetooth antennas on the human tissues.

The study of the interaction between a smartwatch and the individual’s tissues has been carried out through FDTD simulations that allow predicting SAR values. The values obtained are plausible, and so lower than the limits imposed by the regulations in force. Therefore, despite smartwatches are wearable devices, they cannot be considered harmful to the user’s health. Unfortunately, we cannot consider these SAR values as universal values, because each person could have a different sensitivity to radiation exposure.

1. Introduction

1.1 Wearable Devices

Traditionally, data have been collected for special purposes and stored in securely protected databases. In recent years, the word *data* has become a term used daily in our lives and has taken a different meaning: in fact, with the rapid development of web technologies and of the Internet, users are able to generate a vast amounts of data about their daily lives [1].

On the *Internet of Things* (IoT) – the interconnected network of physical devices and other items embedded with electronics that interact with humans or other physical objects and systems, in order to collect and exchange data [2] – the number of connected devices has grown exponentially [1]. Many corporations are spending on IoT technologies, since IoT is leading a revolutionary change in many sectors and businesses, such as manufacturing, retail, energy, agriculture industries, sport and health care [3].

Connected wearables are one of the most adopted IoT systems for personal use. A *wearable device* is a technology that is worn on the human body, often used for tracking a user's vital signs or data related to health and fitness, location and biofeedback [1]. In the broad sense, wearable systems are systems that have one of the following features: wearable, portable, implantable, and ingestible [4]. These products are controlled by electronic components and software and are, generally, connected to smartwatches thanks to short-range wireless systems, such as Bluetooth or local Wi-Fi setups [1]. The most important part of a wearable device is the powerful sensor technology, since sensors are responsible to detect, collect and deliver information about their surroundings [5].

Wearable electronic and photonics have evolved from continuous technological advancements [5]. These devices have been created at the beginning of 60s, when illegal watches have been used in casinos to help players win easier. Between the 70s and 80s, wearable technology has evolved, acquiring a more noble functionality: thanks to companies such as Casio and Citizen, the first wristwatches with additional features, such as stopwatch and calculator, have been introduced on the market. The first wearable hearing aids for the deaf and the first digital viewers were born at the beginning of the 90s; successively, since the 2000s, the wearable device market has grown exponentially, thanks to the birth of new sectors, like that of action cameras, fitness bands and smart glasses [4].

The fast expansion of the use of wearable devices and the extraordinarily growth IoT wearables market can be explained by a number of reasons: first of all, connected wearables are mostly affordable and easy to use devices [5]. Currently, there are many devices that can be classified as wearable devices; for this reason three types of wearable devices – capable of processing data, of communicating with a smart connected device or even of connecting autonomously to the network without relying on other devices – are distinguished [4]:

- *Complex Accessories* are devices created to be able to work only partially independently and that require connection to a smart connected device in order to be operational. This category includes most of the countless bracelets for fitness or for monitoring sports activity;
- *Smart Accessories* are devices that have the possibility to install third-party apps or software; for the full operation of these devices, it is still necessary to connect to a smart device, in turn connected to the internet. Examples of devices of this type are many smartwatches;
- *Smart Wearables* are devices that can work independently, without the need to rely on other devices. They independently connect to the internet and have the ability to install third-party apps and software, with the intention of expanding their functionality.

Wearable solutions are designed for wear on a variety of parts of the body, such as the head, eyes, wrist, waist, hands, fingers, legs, or embedded into different elements of attire. For this reason the IoT solutions are commonly categorised by the body part on which the solution must be worn (*Figure 1*) [6].

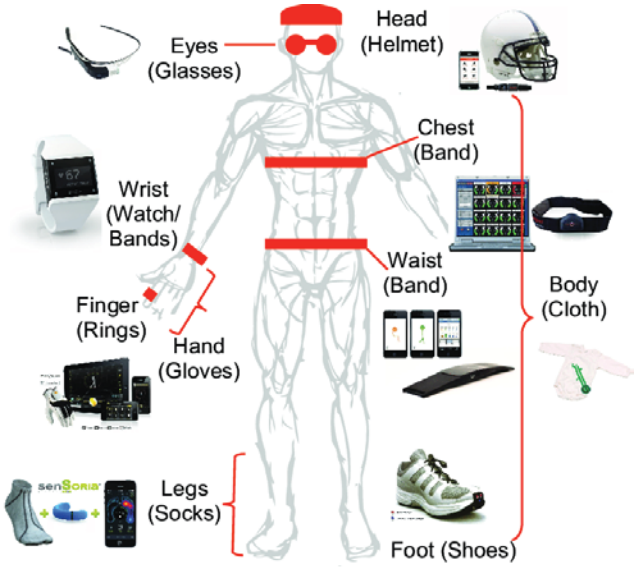

Figure 1: *Wearable Devices [6].*

1.1.1 Smartwatches

Smartwatch is regarded as the first commercialized wearable device for consumers and represents a significant development in the domain of wearable technology [7]. In fact, after several decades of technological development from the initial conception of strapping a computing device to one's wrist, the smartwatch has finally become a viable device that extends the functions of smartphones to a more intimate level [8].

Cecchinato et al. [9] defined a smartwatch as "*a wrist-worn device with computational power, that can connect to other devices via short range wireless connectivity; provides alert notifications; collects personal data through a range of sensors and stores them; and has an integrated clock*". While the earliest models were only able to perform basic operations, such as calculations and translations, most modern smart watches are real wearable computers. In fact, many smart watches run applications, while fewer models have a mobile operating system and function as portable media players. In addition, some smartwatches are called *watch-phones* because they have full network capability and can make or answer calls [10].

While internal hardware varies, the Micro Control Unit (MCU) must coordinate all functions. Sensors are one of the most important parts of a smartwatch, because they are the primary source from which wearable devices collect data: a sensor, in fact, detects data from the surrounding environment and, then, transfers them to the display CPU or processor [11]. Typically, sensors can be divided into three main categories [10]:

- *Motion sensors*: accelerometer, gyroscope, geomagnetic sensor, atmospheric pressure sensor;
- *Biosensors*: includes sensors for detecting parameters such as glucose, blood pressure, ECG, EMG, body temperature;
- *Environmental sensors*: temperature, humidity, gas, PH, ultraviolet, pressure.

Most smartwatches use an Advanced RISC Machines (ARM) architecture. This 32-bit RISC processor architecture, in fact, possess a unique combination of features that makes ARM the most popular embedded architecture today [12]:

- ARM cores are very simple compared to most other general-purpose processors, which means that they can be manufactured using a comparatively small number of transistor;
- Both ARM ISA and pipeline design are aimed at minimising energy consumption;
- The ARM architecture is highly modular;

- While being small and low power, ARM processors provide high performance for embedded applications.

The display is usually touch and can use different technologies; the most used screens in smartwatches are generally of four types [13]:

- *Traditional LCD*: they have higher power consumption and lower contrast ratios;
- *LCD Sharp Memory*: they have excellent visibility and an high refresh rate;
- *E-ink*: perfectly visible under sunlight, they have an high autonomy but they are limited on some technical functions;
- *OLED*: they consume less, have deeper black colours and the elements on the display are clearly visible in sunlight, because they adapt according to the brightness of the environment.

Wireless chipsets are another very important part of a smartwatch: most data transfers are done wirelessly via Bluetooth, Wi-Fi, NFC and GPS that, because of the small size of a smartwatch, are generally integrated [11].

A block scheme of the internal architecture of a smartwatch is represented in the following figure (*Figure 2*).

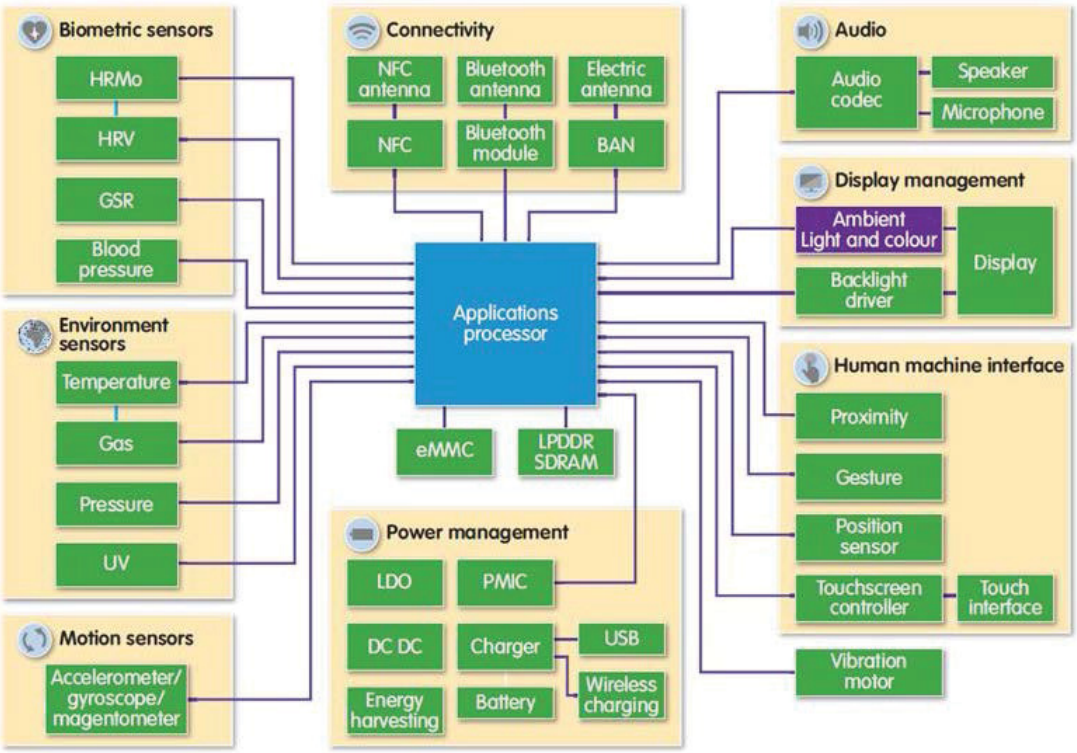

Figure 2: *Smartwatch Block Diagram [12].*

1.2 Device – Human Tissues Interaction

Wearable devices, as all the IoT devices, are used routinely today by the majority of people. Although these technically advanced devices have proved to be of immense benefit – both from the point of view of smart communication and from the point of view of monitoring the daily activities of an individual – their rapid development and continuous improvement have had the unintended consequence of creating a knowledge gap in the study of interactions between the device and human tissues. In fact, while much has been done on the computation of the specific absorption rate (SAR) and standardization of mobile phones, other wearable devices deserve further attention [14].

The main aspect is that they are in direct contact with the human skin so the determination of potential health effects is still an open issue. There is an unmet need to collect existing data on the dynamic and complex process that occurs when devices and human tissues interact. By exploring these areas in detail, engineers can contribute to better understand if wearable devices could be harmful to the user's health, by expanding the collective knowledge base of device-tissue interactions.

1.2.1 Smartwatch Antennas and Electro-Magnetic Frequency Radiation

In order to better understand how smartwatches and human tissues interact, we need to study in detail the correlated radiation transport problem. The *radiation transport problem* bases its foundations on four fundamental concepts [15]:

- *Radiation*: it is the emitted or transmitted energy; it could be an electromagnetic, a particle, an acoustic or a gravitational radiation;
- *Radiation source*: it is the source that emits the radiation;
- *Propagation in matter*: it is the action by which the radiation penetrates through the space or the material medium;
- *Detection*: it is the measure of the emitted or transmitted radiation.

What we tend to forget when we buy smartwatches, is the fact that they emit small amounts of *Electro-Magnetic* (EM) *Radiation*, as all the electronic devices [16]. Thus, a smartwatch can be considered as a radiation source.

During the twentieth century, environmental exposure to man-made sources of Electromagnetic Fields (EMF) steadily increased due to electricity demand, ever-advancing wireless technologies and changes in work practices and social behaviour. Potential health effects of EMF have been a topic of scientific interest since the late 1800s and have received particular attention during the last 30 years [17].

The majority of wearable devices use the Bluetooth (from 2.4 GHz to 2.4835 GHz) or Wi-Fi protocol (2.4 GHz and 5 GHz) [18]; moreover, IoT devices transmit data by using 4G and 5G (and 6G in the future) and the frequencies could be much higher [19].

EMF are much too weak to break the bonds that hold molecules in cells together and, therefore, cannot produce ionization. Thus, the effects on the human body and its cells depend mainly on the EMF intensity and on the duration of the exposure. At radio frequencies, the energy of these fields is partially absorbed and transformed into the movement of molecules: friction between rapidly moving molecules results in a temperature rise. Exposure to low level RF fields (such as those emitted by wearable devices) does not cause adverse health effects; some scientists have reported some minor effects of mobile phone use, like changes in brain activity, reaction times and sleep patterns [17]. More in-depth studies are needed to evaluate the potential health effects of wearable devices.

Since smart wearable devices need the access to wireless data networks, antenna design and RF layout (*Figure 3*) are critical in a wireless system that transmits and receives electromagnetic radiation in free space [20].

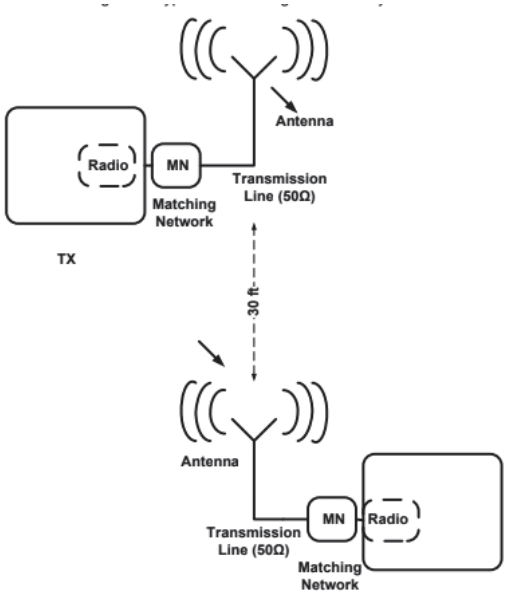

Figure 3: *Typical Short-Range Wireless System [20].*

An antenna is, basically, a conductor exposed in space; if the length of the conductor is a certain ratio or multiple of the wavelength of the signal, it becomes an antenna: this condition is called resonance, as the electrical energy fed to antenna is radiated into free space. When the conductor has a length equal to $\lambda/2$ (*Figure 4*) – λ is the wavelength of the electric signal – the signal generator feeds the antenna (called Dipole Antenna) at its centre point by a transmission line known as antenna feed. At this length, the voltage and current standing waves are formed across the length of the conductor [20].

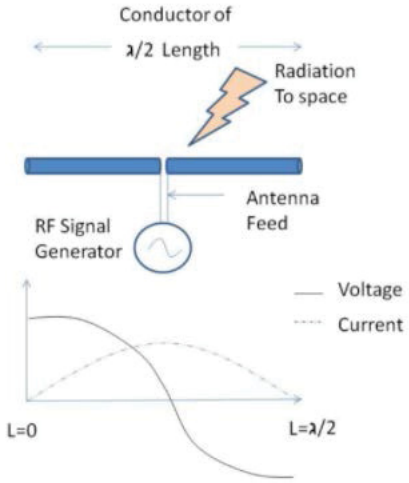

Figure 4: *Dipole Antenna [20].*

Depending on the wavelength, the antenna can be of different dimensions. The selection of an antenna depends on the application, the available board size, cost, RF range, and directivity [20].

However, there are two challenges to wearable devices that make antenna design particularly difficult [21]:

- *Proximity to the Human Body*: the human body is a lossy material for electromagnetic waves; this means the body converts electric fields into heat and absorbs energy from electromagnetic waves. Consequently, when an antenna is placed near the body, the result is a large reduction of the antenna efficiency of your wearable antenna;
- *Very limited Volumes*: wearable devices must be as small as possible. Space is at an extreme premium on wearable devices; as such, industrial designers and product designers often give very little space for the antenna, which further makes the antenna design problem more difficult.

Most PCB antennas fall into the following types [20]:

- *Wire Antenna*: this is a piece of wire extending over the PCB in free space with its length matched to $\lambda/4$ over a ground plane. The wire antenna gives the best performance and RF range because of its dimensions and three-dimensional exposure. This is a three-dimensional (3D) structure, with the antenna over a height of 4-5 mm over the PCB plane, protruding into space;
- *PCB Antenna*: this is a trace drawn on the PCB and can be a straight trace, an inverted F-type trace, a meandered trace, a circular trace or a curve with wiggles depending on the antenna type and space constraints. In a PCB antenna, the antenna becomes a two-dimensional (2D) structure in the same plane of the PCB; it requires more PCB area, has a lower efficiency than the wire antenna, but is cheaper;
- *Chip Antenna*: this is an antenna in a small form-factor IC that has a conductor packed inside. This is useful when there is limited space to print a PCB antenna or support a 3D wire antenna.

Since the smaller the space, the more complex the antenna design is, common practices on the market for the smartwatch antenna designs are the use of the flexible printed circuit board (FPCB) antennas [22].

1.2.2 Human Tissues: Anatomical Overview

The human body is composed of many different types of cells that together create tissues and subsequently organ systems. The wrist joint (also known as the radiocarpal joint) is a synovial joint in the upper limb, marking the area of transition between the forearm and the hand. Anatomically, the wrist joint is formed distally by the proximal row of the *carpal bones* (except the pisiform) and proximally by the distal end of the *radius* and the *articular disk* (*Figure 5*); together, the carpal bones form a convex surface, which articulates with the concave surface of the radius and articular disk [23].

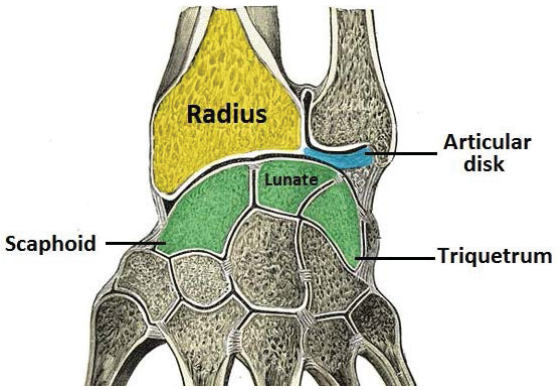

Figure 5: *Articular surfaces of the wrist joint [23].*

Like any synovial joint, there is a dual layered *joint capsule*: the fibrous outer layer attaches to the radius, ulna and the proximal row of the carpal bones; the internal layer is comprised of a synovial membrane, secreting synovial fluid, which lubricates the joint [24].

There are four *ligaments* of note in the wrist joint, one for each side of the joint (*Figure 6*) [25]:

- Palmar radiocarpal: it is found on the palmar (anterior) side of the hand and passes from the radius to both rows of carpal bones. Its function, apart from increasing stability, is to ensure that the hand follows the forearm during supination;
- Dorsal radiocarpal: it is found on the dorsum (posterior) side of the hand and passes from the radius to both rows of carpal bones. It contributes to the stability of the wrist, but also ensures that the hand follows the forearm during pronation;
- Ulnar collateral: it runs from the ulnar styloid process to the triquetrum and pisiform. Works in union with the other collateral ligament to prevent excessive lateral joint displacement;
- Radial collateral: it runs from the radial styloid process to the scaphoid and trapezium. Works in union with the other collateral ligament to prevent excessive lateral joint displacement.

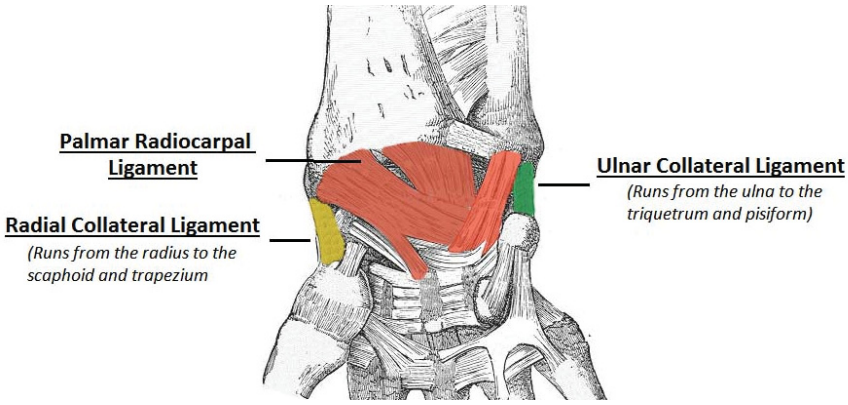

Figure 6: *Palmar view of the ligaments of the wrist joint [23].*

The wrist joint receives blood from branches of the dorsal and palmar carpal arches, which are derived from the ulnar and radial *arteries*. Innervation to the wrist is delivered by branches of three *nerves* [24]:

- Median nerve, the anterior interosseous branch;
- Radial nerve, the posterior interosseous branch;
- Ulnar nerve, the deep and dorsal branches.

The wrist and hand muscles are located primarily in the forearm; often they work synergistically to allow for the dexterity and movement of these joints. The *tendons* of these muscles are longer from the end of the muscle belly to the insertion, and thus require two thick bands at the wrist to anchor them in place [26]:

- The anterior band, known as the Flexor Retinaculum, travels across the palmar side of the wrist and forms the carpal tunnel;
- The posterior band, known as the Extensor Retinaculum, anchors the extensor tendons and assists in supporting the posterior structure of the wrist.

Muscles can by divided by the action they perform (*Figure 7*) [26]:

- Flexion: bending the wrist towards the palm; muscles include Flexor Carpi Ulnaris (prime mover), Flexor Carpi Radialis (prime mover), Palmaris longus (tightens the skin and fascia in the palm), Flexor Digitorum Superficialis (finger flexor, assists only);
- Extension: bending the wrist backwards; muscles include Extensor Carpi Radialis Longus (prime mover), Extensor Carpis Radialis Brevis (prime mover), Extensor Carpi Ulnaris, Extensor Digitorum (assists only);
- Radial Deviation: tilting the hand and wrist toward the thumb and radius; muscles include Flexor Carpi Radialis and Extensor Carpi Radialis (they work together to cancel the flexion and extension and instead just pull toward the radius);
- Ulnar Deviation: tilting the hand and wrist toward the pinky and ulna; muscles include Flexor Carpi Ulnaris and Extensor Carpi Ulnaris (they work together to cancel the flexion and extension and instead just pull toward the ulna).

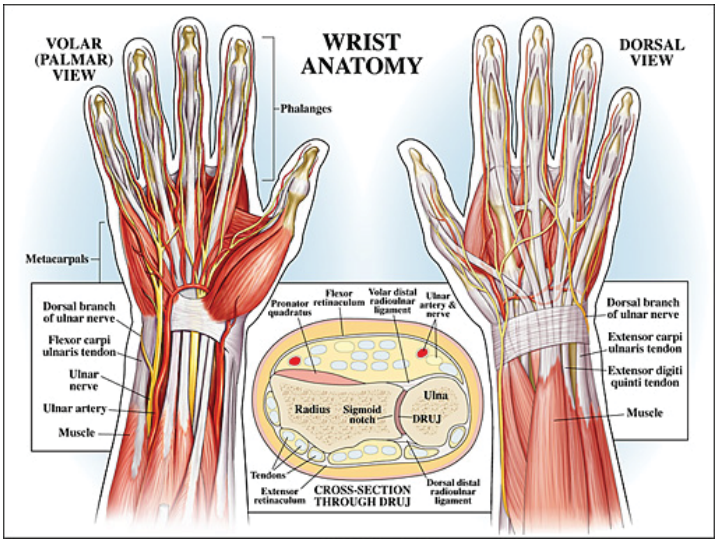

Figure 7: *Wrist Muscles Anatomy* [26].

1.2.2.1 Phantom Models of the Human Body

Since the study of the human body involves anatomy, physiology, histology and embryology, it can be considered a complex science. In order to study the geometry and the anatomy of the human body more easily, *mathematical phantom models* are used; these models serve an important role in several aspects of diagnostic and therapy related image processing [27]. Standardized models of the human body are employed to describe and predict the radiation doses received by various tissues in the body [15]. For internal dosimetry purposes, such human model approximations serve quite sufficiently and have the advantage of allowing very fast calculation of the intersection of ray lines with the analytical surfaces which delineate the organs [27].

Computerized anthropomorphic phantoms could be defined by mathematical (analytical) functions or by digital (voxel-based) volume arrays [27]. Early models representing the human body were mostly homogeneous slabs, cylinders, and spheres. The first heterogeneous anthropomorphic model was devised at Oak Ridge National Laboratory for the Medical Internal Radiation Dose (MIRD) Committee of The Society of Nuclear Medicine. This model, known as MIRD Phantom, was based on the concept of the "Reference Man" for radiation protection purposes, originally defined as being a 20-30 years old Caucasian, weighing 70 kg and 170 cm in height [28]. Later improvements have led to a "family" of models having both sexes at various ages: these MIRD-based models have served practically as the "standard" to the health physics community. Several groups of researchers worldwide, in fact, have used these MIRD-based mathematical models extensively to calculate internal and external organ doses for a variety of health physics applications involving photon, electron, neutron, and proton sources [29]. It is clear, however, that the human anatomy is too complex to be realistically modelled with a limited set of equations; as such, many anatomical details in the mathematical models had to be compromised. The use of advanced imaging techniques – Computed Tomography (CT) and Magnetic Resonance Imaging (MRI) – has allowed developing new realistic body models. Researchers discovered that they could take that diagnostic data and transform it into a voxel (volumetric pixel) format, essentially re-creating the human body in digital form in 3D [30].

Today there are over 38 human phantoms in voxel format, for many different uses; the most famous is the *VoxelMan phantom*, developed by Dr. Zubal and team at Yale University in 1994 [*Available Online: http://noodle.med.yale.edu/zubal/*] [31]. The original phantom consists of a CT-based torso and a CT-based head and has been designed specifically for use in Monte Carlo simulations of nuclear medicine imaging geometries. Successively, it has been improved by Dr. Maria A. Stuchly, who borrowed the arms and legs from the Visible Human and attached them to the original torso phantom (*The Arms Folded Phantom*) [*Available Online:*

http://noodle.med.yale.edu/phantom/getfoldesc.htm]. As a follow-up, Dr. Katarina Sjogreen, straightened the arms out along the phantom's side (*The Arms Down Phantom*) [*Available Online: http://noodle.med.yale.edu/phantom/getdwndesc.htm*].

1.3 Finite-Difference Time-Domain (FDTD)

The *Finite-Difference Time-Domain method* (FDTD) – first proposed by K. Yee – is today's one of the most popular technique for the solution of electromagnetic problems. It has been successfully applied to a wide variety of problems – such as scattering from metal objects and dielectrics, antennas, micro-strip circuits, and electromagnetic absorption in the human body exposed to radiation – thanks to its extremely simple implementation [32].

1.3.1 History and Applications of FDTD

Kane S. Yee first introduced the numerical analysis technique we call the Finite-Difference Time-Domain method in 1966 [32]. To solve an electromagnetic problem, the idea is to apply centered finite difference operators on staggered grids in space and time for each electric and magnetic vector field component in Maxwell's curl equations [32]. The originality of Yee's algorithm resides in the use of finite differences as approximations to both the spatial and temporal derivatives that appear in Ampere's and Faraday's laws [32].

The descriptor "Finite-Difference Time-Domain" and its corresponding "FDTD" acronym were originated by Allen Taflove in 1980 [32]. Since about 1990, FDTD techniques have emerged as primary means to computationally model many scientific and engineering problems dealing with electromagnetic wave interactions with material structures. Current FDTD modeling applications range from near-DC (ultralow-frequency geophysics involving the entire Earth-ionosphere waveguide) through microwaves (radar signature technology, antennas, wireless communications devices, digital interconnects, biomedical imaging/treatment) to visible light (photonic crystals, nanoplasmonics, solitons, and biophotonics) [32].

1.3.2 The FDTD Approach

When Maxwell's differential equations are examined, it can be seen that the change in the E-field in time (the time derivative) is dependent on the change in the H-field across space (the curl) and vice versa. The FDTD method bases its foundations on the following considerations [32]:

- At any point in space, the updated value of the E-field in time is dependent on the stored value of the E-field and the numerical curl of the local distribution of the H-field in space;

- At any point in space, the updated value of the H-field in time is dependent on the stored value of the H-field and the numerical curl of the local distribution of the E-field in space.

This description holds true for 1-D, 2-D, and 3-D FDTD techniques. Yee proposed spatially staggering the vector components of the E-field and H-field into box-shaped cells of a Cartesian computational grid so that the E-components are in the middle of the edges and the H-components are in the centre of the faces. This scheme, now known as a *Yee lattice* (*Figure 8*), has proven to be very robust, and remains at the core of many current FDTD software constructs. *Yee's Algorithm* is able to solve simultaneously the equations for both electric and magnetic fields, using the pair of Maxwell's equations instead of solving individually through an equation wave. [32].

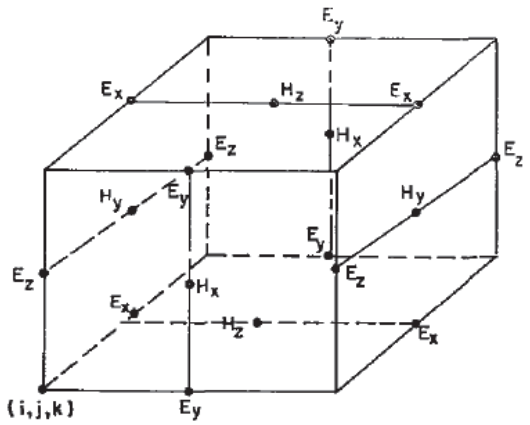

Figure 8: *Illustration of a standard Yee lattice used for FDTD, about which electric and magnetic field vector components are distributed* [32].

In summary, there are three steps in the FDTD computation [32]:

- The discretization of the whole area into small cells (defined as Δx, Δy, and Δz) in the Yee cell;
- The definition of the electrical properties (conductivity and permittivity) of the model in a mesh grid;
- The substitution of partial derivatives by differential quotient in Maxwell's equations (specifically in Ampere's and Faraday's laws).

1.4 Specific Absorption Rate (SAR)

The *Specific Absorption Rate* (SAR) value – expressed in units of power per mass (W/kg) – is a measure of the rate at which radio frequency (RF) energy is absorbed by the human body (or by

a specific mass of the body), under the worst possible circumstances. Thus, SAR provides a straightforward method for evaluating the radiation exposure to our bodies from technological devices, in order to ensure that they are within the safety guidelines set by regulatory bodies, such as the FCC in the US and the CENELEC in the EU [33].

1.4.1 Parameters

Due to the importance of the SAR, it is necessary to evaluate which are the physical quantities that influence the value of the rate and in what way. SAR for electromagnetic energy can be calculated from the electric field within the tissue as [34]:

$$SAR = \frac{1}{V}\int_{sample}\frac{\sigma(r)|\boldsymbol{E}(\boldsymbol{r})|^2}{\rho(r)}dr$$

where σ, ρ and V are, respectively, the electrical conductivity, the density and the volume of the biological tissue and $|E|$ is the maximal value of the electric field induced in the human body. SAR is generally averaged either over the whole body, or over a small sample volume (typically 1 g or 10 g of tissue) [33].

It is easy to see that the SAR is directly proportional to the electrical conductivity of the material in examination and therefore strictly dependent on the geometric characteristics of the space involved in the emission of electromagnetic waves. In fact, the electrical conductivity depends, among other things, on the length and area of the cross section of the section considered. In addition, the SAR is directly proportional to the square of the effective value (Root Mean Square) of the intensity of the electric field. The SAR is inversely proportional to the density of the material that the field radiates. Since the geometric characteristics and the density of the human tissues are very different respect to other materials, it is clear that the SAR calculation will not be uniform over the whole region in which the power is emitted by the E field. In fact, SAR will vary significantly between one tissue and another and also within the same tissue, from one point of the space to the other [34].

SAR also depends on the following parameters [33]:

- The parameters connected with the incident field (intensity, frequency, polarization and configuration of the irradiated sample with respect to the field, near and far field conditions);
- The dielectric properties of the various thicknesses of tissues crossed and the effects of earth and reflection of other bodies present in the irradiation field.

1.4.2 Regulations

Strong electrical and magnetic radiation has been proven as harmful to human health. As a result many countries and regions have published RF exposure standards and regulations, including the SAR levels applicable to mobile telecommunications equipment. Thus, SAR testing is required for type approval of mobile phones in most countries [33].

The SAR rating was first introduced in regulations in 1996, when the Federal Communication Commission released specific guidelines on human exposure to cell phone radiation. They created SAR as a mean of measuring how much RF your body can take when making a call: the outcome of these proceedings was that a person cannot absorb more than 1.6 watts of energy per kilogram of body weight. This upper limit of specific absorption rate is set well below the level of radiation that would endanger a user's health [33].

The ICNIRP (International Committee for Non-Ionizing Radiation Protection) is the independent organization to which the World Health Organization refers to establish the fundamental guidelines. These limits are equal to [33]:

- 2.0 W/kg in Europe, where the regulations are established by CENELEC (European Committee for Electrotechnical Standardization) and the SAR is calculated over a period of 6 minutes and averaged over 10 grams of tissue;
- 1.6 W/kg in the USA, where the regulations are established by the FCC (Federal Communication Commission) and the SAR is averaged over 1 gram of tissue.

The limit of SAR for wearables devices is generally set to 4.0 W/kg averaged over 10 grams if we refer this measure to limbs [33].

1.4.3 Dosimetry

Radiation dosimetry in the fields of health physics and radiation protection is the measurement, calculation and assessment of the ionizing radiation dose absorbed by an object, usually the human body. Thus, the term dosimetry indicates the determination of the dose of power absorbed by a body exposed to an electromagnetic field, gradually varying the different conditions of exposure [33].

Electro-Magnetic Field dosimetry is a good starting point for evaluating the possible effects they have on biological systems [35]. The choice of SAR as a cardinal parameter in the dosimetric study arises from its use in regulations as a parameter to establish the risk deriving from exposure. Its use in regulations derives, in turn, from the fact that the SAR mediated over the whole body and

the local SAR are ideal for a comparison of observed effects under different exposure conditions [33].

The SAR distribution can be evaluated from numerical and experimental point of view [36]:

- The numerical dosimetric study analyzes the power absorption from a purely theoretical point of view starting from appropriate models of EM field sources and the human body. This is precisely the approach it uses numerical methods such as the Method of Moments (MoM) and the method of Finite Differences in the Time Domain (FDTD);
- The measurements of the induced field inside the body starts from real sources and creates the dielectric models that emulate the human body.

Dosimetric studies indirectly evaluate the effects of the thermal power absorbed by the body (or by individual parts) in the different tissues, since SAR is directly linked to the temperature increase and the link is represented by the bio-heat equation [36].

1.4.4 Types of SAR Calculation

The calculation of SAR can be performed in different ways. The first classification that we can make in the SAR calculation depends on the position of the electromagnetic field source (radio frequency) when considering the exposure of the human body [37]:

- The *whole-body-average* SAR – the SAR analysed on the whole human body – is evaluated when considering the exposure to a far-field source (far-field exposure);
- The *body-part* or *organ-average* SAR – the SAR analysed on specific anatomical parts – is evaluated when considering the exposure to a far-field source, with respect to precise areas and especially when considering a near or intermediate field source and the body partially exposed;
- The *local-average* SAR is evaluated when considering the exposure of a specific part of the body to a near-field source that works at radio frequencies and at a very close distance to the part considered.

The local-average SAR can be averaged over different mass (and volume) quantities [33]:

- The *punctual SAR* calculates the rate of each single Yee cell contained in the computation space;
- The *averaged SAR* instead calculates the average absorption rate of a set of Yee cells such as to reach the total weight of 1 gram (SAR averaged over 1 gram) or 10 grams (SAR

averaged over 10 grams) and it is done for each group of contiguous cells belonging to the examined space.

1.5 Electrical Properties of Tissues and Cole-Cole Equation

The electrical properties of non-excitable tissues are of considerable importance for a large number of bioelectrical phenomena; in fact, they determine the paths of the current flow through the body and, thus, becoming fundamental in various fields of biomedical investigation [38].

An in-depth knowledge of the electrical properties of biological tissues is clearly required in electromagnetic dosimetry, where simulations of exposure to electromagnetic sources are carried out for the calculation of the internal fields of biological structures. As already mentioned, the calculation is carried out through the use of high resolution anatomical models, where the relative electrical properties are assigned to the various tissues for all frequencies to which the model is exposed [36].

The electrical properties of tissues can be described in terms of the *complex dielectric permittivity* of a lossy dielectric material, expressed as [39]:

$$\varepsilon^*_{r_{eff}}(\omega) = \varepsilon'_r(\omega) - j\left(\varepsilon''_r(\omega) + \frac{\sigma_{dc}}{\omega\varepsilon_0}\right) = \varepsilon'_r(\omega) - j\left(\frac{\sigma_{ac}(\omega) + \sigma_{dc}}{\omega\varepsilon_0}\right)$$

The *electrical conductivity of the medium* is identified by the following quantity [39]:

$$\sigma(\omega) = \sigma_{ac}(\omega) + \sigma_{dc} = \omega\varepsilon_0\varepsilon''_r(\omega) + \sigma_{dc}$$

It consists of two contributions: σ_{dc} (continuous) which represents the ohmic conductivity (deriving from the mobility of the ionic species present in a specific tissue) and σ_{ac} (alternating) due to losses due to dielectric relaxation [39].

As the frequency increases, the permittivity of a tissue typically decreases, according to at least three main steps known as [40]:

- Relaxation α;
- Relaxation β;
- Relaxation Υ.

Each relaxation is characterized by its own time constant τ (*dielectric relaxation constant*). It should be noted that for some tissues they may not be clearly distinguishable and furthermore there may be further secondary relaxations [40].

Each of these characteristic times can be placed in relation to a model that includes the following *Debye Equation* for the complex relative permittivity [40]:

$$\varepsilon_r^* = \varepsilon_\infty + \frac{\varepsilon_s - \varepsilon_\infty}{1 + j\omega\tau}$$

Where ε_∞ is the permittivity at frequencies for which $\omega\tau >> 1$, while ε_s is the permittivity at frequencies for which $\omega\tau << 1$.

The complexity of both the structure and composition of biological tissues is such that each dispersive region can be extended by multiple contributions [38]. This extension can be contemplated empirically by introducing a distribution parameter α, used to modify the Debye expression according to the *Cole-Cole Equation*. In general, therefore, the spectrum of a tissue can be more appropriately described in terms of multiple relaxations of the Cole-Cole type [41]:

$$\varepsilon_{r_{eff}}^*(\omega) = \varepsilon_\infty + \sum_n \frac{\Delta\varepsilon_n}{1 + (j\omega\tau_n)^{(1-\alpha_n)}} + \frac{\sigma_{dc}}{j\omega\varepsilon_0}$$

Where the extent of the dispersion is described by $\Delta\varepsilon = \varepsilon_s - \varepsilon_\infty$.

1.6 Previous Studies and Aim

The great interest in the world of smartwatches has led to an increase in academic research [8]. Nevertheless, the majority of studies on wearable devices did not restrict the research subject to a specific type of smart wearable devices; moreover, most of the studies on smartwatches have been focused on the usability, the perceived value, and the fashion perception of them [11]. In addition, there is a significant literature production focused on how smartwatches can be utilized for various purposes, like healthcare, fitness tracking and biometric sensors. Examples are the studies conducted to verify the smartwatches performance in detect atrial fibrillations (J.M. Bumgarner et al. [42] or J. Wasserlauf et al. [43]) or to prove the usability of smartwatches in real time collection of pain scores (T.M. Manini et al. [44]).

Since these devices are in close contact with the human body and continuously emit a small amount of EMF radiation [16], the question is if they could be harmful to the user's health. Currently, there is no significant research aimed at studying interactions between the device and human tissues.

Therefore, in order to fill in the aforementioned gap in research, the purpose of this study is the electromagnetic characterization of the wrist, useful for the determination, through FDTD

simulations, of the effects of the electromagnetic fields generated by Bluetooth antennas on the human tissues. The study of the interaction between a smartwatch and the individual's tissues has been carried out through FDTD simulations that allow predicting electric field strength and SAR values.

2. Materials and Methods

The study of the interaction between a smartwatch and the individual's tissues has been carried out through FDTD simulations, that allow predicting electric field strength and SAR values.

In order to understand the methods that have been applied, a summary block diagram has been created (*Figure 9*); as it is possible to see, light blue rectangles represent the procedure applied and the light green circles represent the respective results. The first phase is the *Choice of a Model* that correctly describes the relative position, the relative orientation and the electrical properties of the tissues of the wrist. The second phase relates to the *Opening of the file in C programming language* and the consequent *Extrapolation of Data*. Therefore, the use of the *ParaView Software* allowed the representation and visualization of the 3D model of the wrist; here, it is possible to apply the dipole representing the Bluetooth antenna of the smartwatch (*Modelling of the Dipole*). Finally, the creation of an homemade Finite Difference Time Domain (FDTD) code, in order to compute the electromagnetic field inside the body phantom (*FDTD Simulation*).

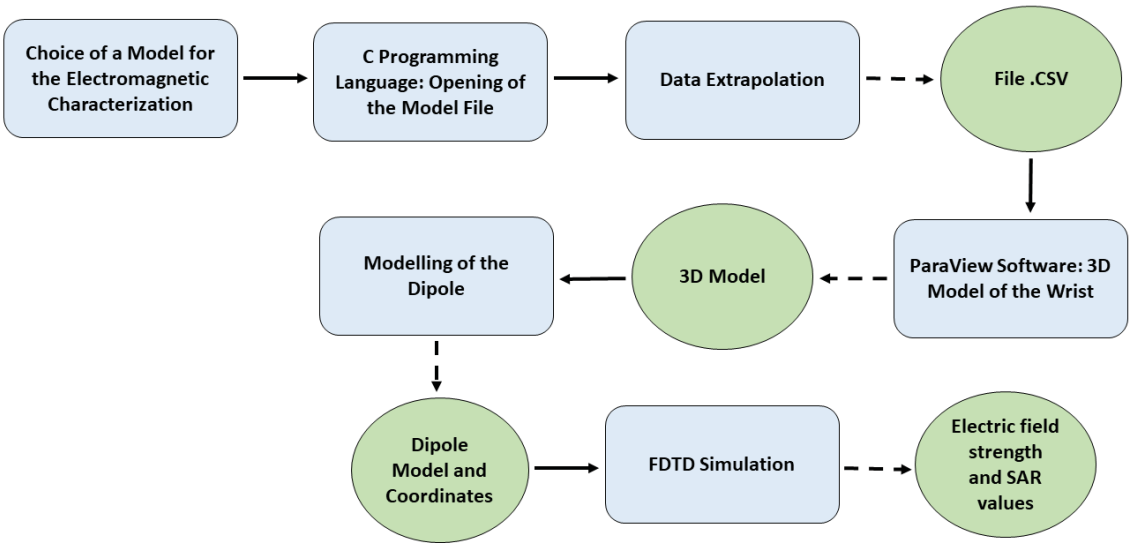

Figure 9: *Methods Block Diagram.*

2.1 Choice of a Model for the Electromagnetic Characterization

To perform FDTD simulations on specific portions of the human body, it is necessary a model that correctly describes the relative position, the relative orientation and the properties of the tissues of the wrist.

The model developed by Professor Maria A. Stuchly from the Department of Electrical and Computer Engineering of the University of Victoria Engineering has been chosen [*Available*

Online: http://noodle.med.yale.edu/phantom/getfoldesc.htm]. The *Arms Folded Model* is a modified version of the Zubal Voxel phantom and consists of 493x87x147 voxel elements, with a size of 3.6x3.6x3.6 mm^3 each. It has been created from the following:

- The Zubal torso with 3.6 mm resolution;
- The Zubal head of 3.6 mm resized to fit the torso;
- Zubal brain of 1.2 mm resolution resampled onto 3.6 mm grid;
- Arms and legs segmented from Visible Man red color crossections;
- Taken with 5 mm space between samples and resampled onto 3.6 mm grid.

In this model, the blood vessels in the arms and legs has been drawn manually using a body atlas; in addition, a single layer of skin has been applied to the outside of the body (each tissue voxel touching air with one of the sides converted to the skin type).

The *Arms Folded Model* is presented in a ".DAT" format, so as a binary file containing all the necessary information relating to the model, that is represented in ASCII, where each character corresponds to a specific tissue. Opening the file through a normal text reader capable of converting the file from binary to text, you can see 147 sections consisting of 493 lines, each containing 87 characters.

To open and use this file it is necessary to use the C programming language, that – thanks to its high versatility – allows the reading and management of most formats, through the correct implementation of the instructions in code.

2.2 C Programming Language: Opening of the Model File

In order to correctly open the file and load it onto an array, the first thing to do is identify its size. The identification of the file size – essential in order to allocate the correct amount of memory without waste – has been carried out using the following sequence of instructions:

```
fseek (file, 0, SEEK_END);

fileLen = ftell (file);

fseek (file, 0, SEEK_SET);
```

Then, the entire file has been allocated within a one-dimensional array (buffer), whose size is defined by a dynamic allocation thanks to the preceding code strings:

*buffer = (char *) malloc (fileLen + 1);*

The file has been read through the following instruction:

fread (buffer, fileLen, sizeof (int8_t), file);

Once the file has been correctly read and loaded onto a one-dimensional array, it has been transferred – through an iteration of three "for" loops – to a dynamic three-dimensional array with a size of 493x87x147, in order to obtain the correct arrangement of the ASCII characters. Each character will have coordinates i, j, k (which correspond to the counter variables of the for loops) with:

$$0 \leq k \leq 493$$

$$0 \leq j \leq 87$$

$$0 \leq i \leq 147$$

This representation allows to map each point constituting the model and, consequently, to obtain a three-dimensional representation.

2.3 Data Extrapolation

Once the model has been implemented in the C programming environment, it is possible to extrapolate the useful data, in order to lay the foundations for the FDTD simulation. A function of the C code reads the “int” array of human body geometry and assigns to each identification number a tissue; the tissue names and their densities ρ are reported in *Table 1*.

Table 1: *Tissues of interest and their related density*

#	Tissue	Density (kg/m^3)
0	Air	1.14
1	Blood	1049.75
2	Bone (Cortical)	1908.00
3	Bone Marrow (Nor Infiltrated)	1099.50
4	Cartilage	1099.50
5	Fat (Not Infiltrated)	911.00

6	Muscle	1090.40
7	Nerve	1075.00
8	Skin (Dry)	1109.00

By resorting to the "*switch-case-default*" control structure a correlation between the human body tissues and their electrical properties has been obtained; each number following the "case" structure represents the ASCII code of the character relating to a specific tissue (87 characters representing 87 different tissues). However, it has been noted that many of these tissues had similar if not identical dielectric properties. Thus, a new matrix – called "*reduced_marix*" – has been created; here the tissues with equivalent dielectric properties are grouped, in order to simplify the model. The selected relevant tissues with the corresponding dielectric properties are reported on *Table 2*; this table will later be used in the Cole-Cole equation.

Table 2: *Parameters to evaluate for the wrist tissues*

#	ε_∞ (F/m)	$\Delta\varepsilon_1$ (F/m)	τ_1 (ps)	α_1	$\Delta\varepsilon_2$ (F/m)	τ_2 (ns)	α_2	$\sigma_{1\text{-}4}$ (S/m)	$\Delta\varepsilon_3$ (F/m)	τ_3 (µs)	α_3	$\Delta\varepsilon_4$ (F/m)	τ_4 (ms)	α_4
0	1.0	0.0	0.0	0.0	0.0	0.0	0.0	0.0	0.0	0.0	0.0	0.0	0.0	0.0
1	4.000	56.00	8.377	0.100	5200	132.629	0.100	0.700	0.00E+0	159.155	0.200	0.00E+0	15.915	0.000
2	2.500	10.00	13.263	0.200	180	79.577	0.200	0.020	5.00E+3	159.155	0.200	1.00E+5	15.915	0.000
3	2.500	3.00	7.958	0.200	25	15.915	0.100	0.001	5.00E+3	1591.549	0.100	2.00E+6	15.915	0.100
4	4.000	38.00	13.263	0.150	2500	144.686	0.150	0.150	1.00E+5	318.310	0.100	4.00E+7	15.915	0.000
5	2.500	3.00	7.958	0.200	15	15.915	0.100	0.010	3.30E+4	159.155	0.050	1.00E+7	7.958	0.010
6	4.000	50.00	7.234	0.100	7000	353.678	0.100	0.200	1.20E+6	318.310	0.100	2.50E+7	2.274	0.000
7	4.000	26.00	7.958	0.100	500	106.103	0.150	0.006	7.00E+4	15.915	0.200	4.00E+7	15.915	0.000
8	4.000	32.00	7.234	0.000	1100	32.481	0.200	0.000	0.00E+0	159.155	0.200	0.00E+0	15.915	0.200

where 0 = Air, 1 = Blood, 2 = Bone (Cortical), 3 = Bone Marrow (Nor Infiltrated), 4 = Cartilage, 5 = Fat (Not Infiltrated), 6 = Muscle, 7 = Nerve, 8 = Skin (Dry).

2.4 ParaView Software: 3D Model of the Wrist

As previously discussed, a three-dimensional matrix useful for providing the position of each tissue element has been obtained; being a 493x87x147 matrix we will have to deal with 6,304,977 tissue elements, each in its i, j, k coordinates.

In order to visualize all points in a 3D space, the *ParaView Software* has been used. ParaView is an open-source cross-platform software, originated in the 2000s by the collaboration of Kitware inc. and Los Alamos National Laboratory, through funds provided by the US Department of Energy ASCI Views program. Thanks to its high versatility, it is often used in the scientific

community for the study of both quantitative and qualitative level [*ParaView overview available online: https://www.paraview.org/overview/*]. The following figure represents a basic screen of the ParaView Software (*Figure 10*).

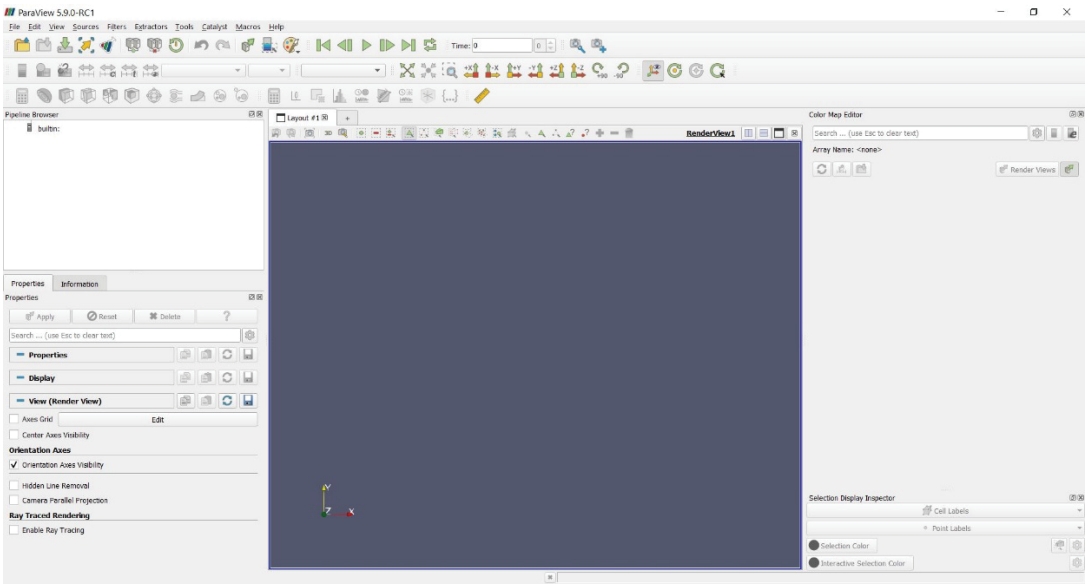

Figure 10: *Basic Screen of the ParaView Software.*

For the correct representation of the 3D model of the wrist in ParaView, it is necessary to change the model from C to ParaView; in fact, ParaView only reads certain types of formats. The format chosen for the display the 3D representation is ".csv", generated directly via C using the following code strings:

*//Writing a *.csv file about head geometry*

// Format:ix, iy, iz, i_scalar_value

sprintf (srsim, "./GEOMETRY_%s%.3d.csv", PREFIX_SIM, LABEL_SIM);

printf ("Opening the file: %s\n", srsim);

The file generated starting from the initial matrix in C, is a file containing respectively the coordinates i, j, k of the points making up the model and the scalar value of each point corresponding to an ASCII code character representing the relative tissue.

By correctly loading the file on ParaView and indicating to the software which of i, j, k corresponds to the Cartesian axes X, Y, Z in space, the model transfer is successfully obtained. By applying some filters (*Filters → Alphabetical → Extract Location*), it is possible to translate the points into a 3D model, as shown in *Figure 11*.

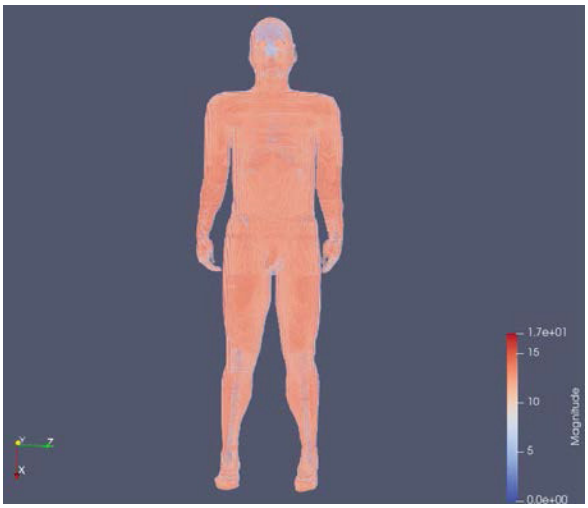

Figure 11: *3D Representation of the Human Body.*

The 3D image displayed on ParaView represents the entire human body; thus, since we are only interested in the wrist, we have to extract the forearm area. In order to do this, a sort of parallelepiped has been constructed around the area of interest in the right arm (*Figure 12*) and the correlated coordinates of the vertices (8 points) has been noted (*Table 3*).

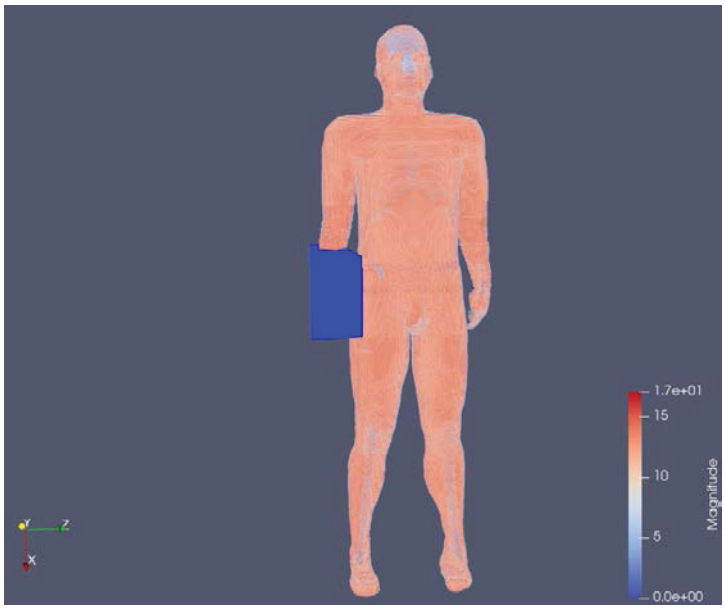

Figure 12: *Parallelepiped construction around the area of interest.*

Table 3: *Coordinates of the Vertices of the Parallelepiped*

Point	X	Y	Z
P1	623.234	0.599781	16.3102
P2	627.925	0.0990495	109.753

P3	935.075	5.15301	9.68289
P4	934.263	5.15045	111.282
P5	592.555	247.556	3.84008
P6	589.103	247.908	78.413
P7	941.501	246.416	4.77679
P8	939.775	242.582	79.3562

Now, it is important to intervene through the C programming environment in order to extract the area of interest and simplify the model, using the coordinates of the vertices of the parallelepiped. We proceeded, as before, with the extrapolation of the coordinates and the reimplementation of the model in ParaView; the result is shown in *Figure 13*.

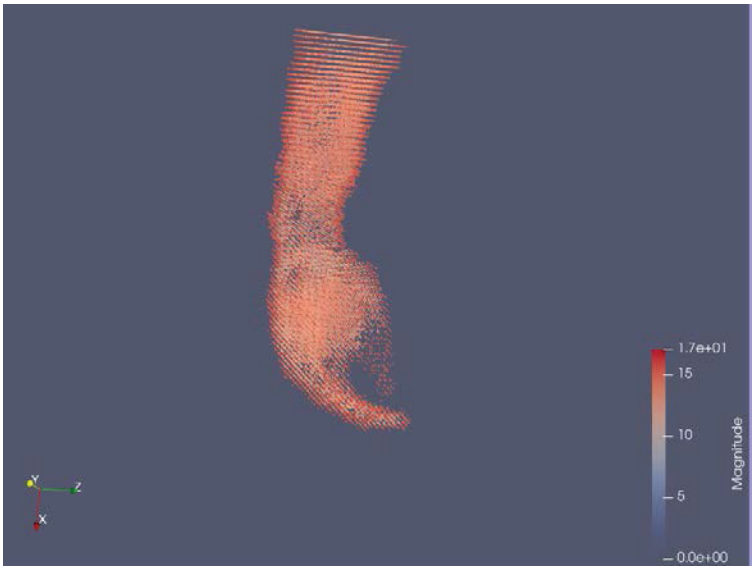

Figure 13: *3D Representation of the Forearm.*

2.5 Modelling of the Dipole

The purpose of this study is the electromagnetic characterization of the wrist, useful for the determination, through FDTD simulations, of the effects of the electromagnetic fields generated by Bluetooth antennas on the human tissues.

In order to simulate the electromagnetic fields, we have to simulate the presence of a smartwatch. For this reason, the Arbily ID205L Smartwatch (*Figure 14*) has been chosen as a reference model; the product parameters are shown in *Table 4*:

Table 4: *Arbily ID205L Smartwatch Parameters*

Model	ID205L	**Screen type**	1.3-inch color screen
Battery capacity	210 mAh	**Charging Voltage**	5 V ± 0.2 V
Charging Time	About 2.5 hours	**Battery Life**	Over 10 days
Waterproof Level	5 ATM	**Weight of Product**	38 g
Operating Temperature	- 20 °C – 40 °C	**Bluetooth Version**	BLE 4.2
Product Frequency	2402 – 2480 MHz	**Max. Transmission Power Consumption**	0 dBm

Figure 14: *Arbily ID205L Smartwatch.*

What we want to simulate is the Bluetooth antenna of the smartwatch device: for this reason, we have chosen a specific model of dipolar antenna (*Figure 15*), which will be positioned exactly on the wrist of the model implemented on ParaView (*Figure 16*). Thus, in order to obtain the spatial coordinates where the dipole will be positioned, the "Extract Location" filter has been used; the coordinates are:

$$X = 811.78$$

$$Y = 121.503$$

$$Z = 4.83175$$

Where the three Cartesian axes X, Y, Z are oriented as follows:

- X from the wrist down (fingers);
- Y from the wrist outwards;
- Z from the wrist inwards.

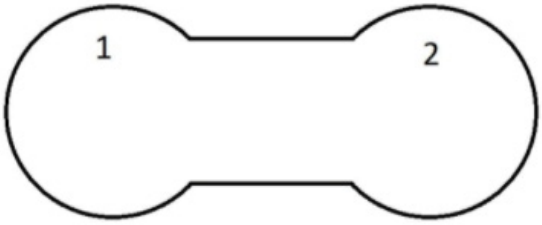

Figure 15: *Dipole representing the antenna; the poles are numbered.*

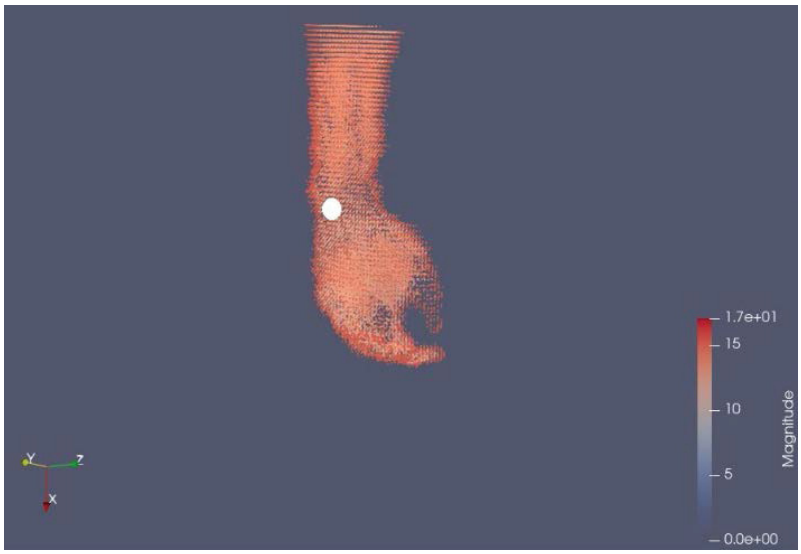

Figure 16: *The point of application of the dipole (white circle).*

2.6 FDTD Simulation

The study of the interaction between the smartwatch and the individual's tissues has been carried out through FDTD simulations that allow predicting electric field strength and SAR values. In fact, the purpose of carrying out simulations is to have a confirmation of how the SAR varies in terms of numerical value and range of values within the cells that make up the simulation environment.

As already mentioned, the antenna has been characterized as a folded dipole 2.6 cm long. The dipole is connected to a transmission line, simulated with an FDTD-1D domain. The transmission line has a characteristic impedance Z_0 of 51.6 ohms and the power incident on the transmission line is normalized to 1 W. The right side is ended on the 3D domain where the folded dipole is

located; the other side, instead, is ended on an adapted load equal to its own characteristic impedance. Thus, on the right of the separation surface, the incident voltage is added to the voltage calculated with the FDTD-1D in order to obtain the total voltage; on the left, the incident current is subtracted from the current calculated with the FDTD-1D in order to obtain only the reflected current. The cell-by-cell calculation process has been carried out using a code implemented with the C programming language.

This model allows to calculate the value of the electric field (E), the magnetic field (H), the current (I) and the voltage (V), through the union of the FDTD-1D and FDTD-3D domains. In fact, the FDTD-1D grid simulating the transmission line and the FDTD-3D grid simulating the forearm are connected at the end of the transmission line and at the centre of the folded dipole.

The majority of wearable devices use the Bluetooth or Wi-Fi protocol [18]; for this reason, we choose f = 2.45 GHz for the FDTD simulations. In particular, we adopted a standard FDTD algorithm with sinusoidal excitation.

The first step to proceed with the simulation is the calculation of σ and ε_r related to each of the tissues of interest (at the frequency of 2.45 GHz). The complex dielectric constant $\varepsilon(\omega)$ of each FDTD cell is is a summation of four Cole-Cole expressions:

$$\varepsilon(\omega) = \varepsilon_\infty + \sum_{m=1}^{4} \frac{\Delta\varepsilon_m}{1 + (j\omega\tau_m)^{(1-\alpha_m)}} + \frac{\sigma_i}{j\omega\varepsilon_0}$$

where $\omega = 2\pi f$ and $\varepsilon_0 = 8.854 \cdot 10 - 12\ F/m$ is the permittivity of free space and the parameters to compute the complex dielectric constant for a fixed frequency in the band $10\ Hz < f < 100\ GHz$ are those reported in *Table 2*.

Table 5 reports the tissue number and name, the relative dielectric constant and the conductivity, for the frequency $f = 2.45\ GHz$ and the temperature $T = 37°C$.

Table 5: *Dielectric Constants and Conductivity of Tissues*

#	ε_r	σ (S/m)
0	1	0
1	58.26	2.545
2	11.38	0.3943
3	5.297	0.09554
4	48.91	1.808

5	5.280	0.1045
6	52.73	1.739
7	30.15	1.089
8	38.01	1.464

Therefore, the simulation has been carried out using the FDTD method, so we must consider the weaknesses of the FDTD approach [32]: the main limitation is the need to divide the entire computational domain into grids. Thus, the spatial discretization of the grids must be good enough to solve both the smallest electromagnetic wavelengths and the smallest geometric element of the considered model: this results in the development of a very wide computational domain. For this reason, there are a large number of boundary absorption conditions that can be used to simulate an unlimited computational domain very effectively. The two most suitable methods for this purpose are [32]:

- The *Perfectly Matched Layer* (PML), a technique developed by Berenger in 1994 which involves the use of an absorption material outside the computing space capable of decomposing the EM wave if it exceeds the limits;
- The *Boundary Absorption Conditions of MUR*, proposed and developed by G. Mur since 1981. The implementation of these conditions is simpler than that of the PML; however, this method causes a large error in certain regions of space and, therefore, the PML technique is generally used in order to guarantee greater accuracy.

Thus, in order to obtain the value of the averaged SAR within the model, a cell of the forearm has been firstly considered; then, the layers around this cell has been gradually added, up to a total weight of 1 gram and 10 grams. The methodology has been iterated for all the cells inside the forearm made of a human tissue and not of air (i.e. not belonging to the empty cavities present). A code in the C programming language (procedure "*cell_add*") has been implemented: it adds a contiguous cell to the starting cell and modifies all the parameters that depend on the number and entity of the cells, such as the current mass, the average SAR and the number of cells considered.

void

*cell_add (struct_grid * grid, struct_geobody * body, double *weight, double*

****sar, double *sar_averaged _volume, double*

**sar_averaged _weight, long int *n_cells,*

```
int i, int j, int k)

{

double actual_weight;

actual_weight = grid->dx[i] * grid->dy[j] * grid->dz[k] * body-

>density[body->tissue [i][j][k]];

*weight += actual_weight;

* sar_averaged _volume += sar[i][j][k];

* sar_averaged _weight += sar[i][j][k] * actual_weight;

*n_cells = *n_cells + 1;

}
```

Subsequently, the variables – as the generic coordinates of the initial cell and those of the cell that are added – have been declared; furthermore, the quantities to be measured – the number of cells examined and their total weight and the averaged SAR – are initialized to zero. The triple "for loop" has the purpose of iterating the instructions for all the voxel elements of the model, while the last line contains an "if" condition which ensures that the starting cell chosen is not composed of air (in fact the number '0' identifies the "air"):

```
for (k0 = 0; k0 < body->dim_k; k0++)

for (j0 = 0; j0 < body->dim_j; j0++)

for (i0 = 0; i0 < body->dim_i; i0++)

{

if (body->tissue[i0][j0][k0] > 0)
```

Once the initial cell satisfies the condition, it is necessary to update the quantities that have been initialized to zero; thus:

- The weight of the initial cell is defined as the product of the infinitesimal volume of the initial cell times the density of its tissue;
- The averaged SAR over volume is increased by the cell's punctual SAR value;

- The averaged SAR over weight is calculated as the product of the first times the weight.

The code provides the gradual addition of cells around the starting one; this crucial part of the code is divided in turn in three parts. The cells are, therefore, divided into three types:

- The cells at the top of the "cube" that is created (for the first layer are 8);
- The cells on the edges that are not vertices (are 12);
- The cells centered on each of the six faces of the "cube".

It has been estimated that this choice facilitates the addition of cells in the layer around the starting one. In fact, the division into three parts makes the total weight of the cells more controllable, especially when the layers begin to be numerous and the number of edges and faces increase with cubic proportion. It is possible to reach the maximum weight (1 g or 10 g) in an intermediate point of the layer; thus, the control of the weight accumulated before is extremely important in avoiding that the "*weight_max*" limit is greatly over-exceeded.

The "*cell_add*" procedure is used for the addition of each Yee cell, but it does not calculate the average of the punctual SAR value of each cell. The *averaged SAR over volume* is obtained as the ratio between the sum of the punctual SAR of the individual cells considered and the number of the cells; the *averaged SAR over weight* is calculated as the ratio between of the punctual SAR of the individual cells and the final weight (therefore for 1 or 10 grams).

```
sar_averaged _volume /= (double) n_cells;

sar_averaged _weight /= weight;

}

else

{

sar_averaged _volume = (double) 0;

sar_averaged _weight = (double) 0;

}
```

It is important to verify that the averaged SAR value complies with the limits imposed by the regulations in force, thus [33]:

- 2.0 W/kg in Europe, where the SAR is calculated over a period of 6 minutes and averaged over 10 grams of tissue;
- 1.6 W/kg in the USA, where the SAR is averaged over 10 grams of contiguous tissue.

In addition, the limit of SAR for wearables devices is generally set to 4.0 W/kg averaged over 10 grams if we refer this measure to limbs [33].

Therefore, it is very useful to add a last part in the C code, in order to identify the maximum value of the SAR averaged over 1 or 10 grams to verify that the different conditions of exposure of the wrist to the electromagnetic fields produced by the smartwatch antenna does not exceed the threshold values imposed by the regulations.

printf ("Max Value of the Averaged SAR %g W/kg (%d, %d,%d).

The value has been calculated over the weight.\n", sar_averaged _max_weight,

i0_max_weight, j0_max_weight, k0_max_weight);

printf ("Max Value of the Averaged SAR %g W/kg (%d, %d,%d).

The value has been calculated over the volume.\n", sar_averaged_max_volume,

i0_max_volume, j0_max_volume, k0_max_volume);

3. Results

FDTD calculations have been performed in order to investigate the effects of the electromagnetic fields generated by Bluetooth antennas on the human tissues; FDTD simulations, in fact, allow predicting electric field strength and SAR values.

In our simulation, the following results have been obtained:

- The maximum value of SAR mediated over 1 gram and over the weight is equal to 0.453 W/kg;
- The maximum value of SAR mediated over 1 gram and over the volume is equal to 0.334 W/kg;
- The maximum value of SAR mediated over 10 grams and over the weight is equal to 0.203 W/kg;
- The maximum value of SAR mediated over 10 grams and over the volume is equal to 0.159 W/kg.

The results are reported in the following table (*Table 6*).

Table 6: *SAR Values obtained from FDTD Simulation*

Total weight	Averaged SAR over weight	Averaged SAR over volume
1 g	0.453 W/kg	0.334 W/kg
10 g	0.203 W/kg	0.159 W/kg

For a best visualization of the SAR values obtained and in order to more clearly discuss the results, the histogram representation is proposed in *Figure 17*. Thanks this graphic representation, in fact, it's easy to compare the values obtained for the averaged SAR over weight and the averaged SAR over volume, both for a total weight of 1 g and 10 g.

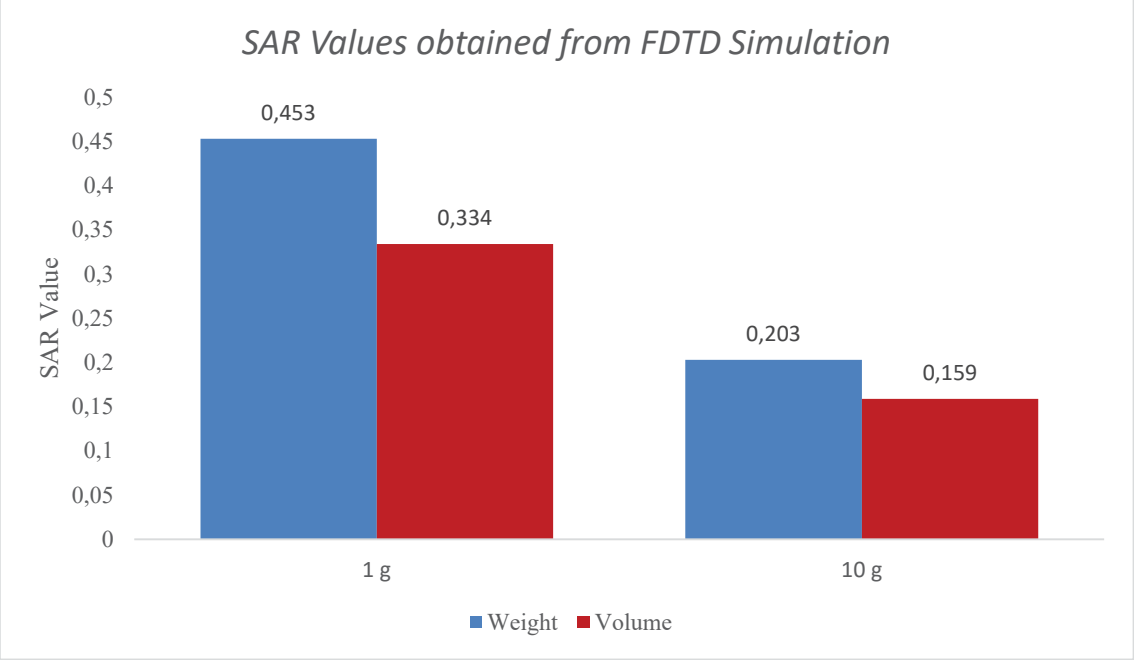

Figure 17: *1 and 10 g SAR Values obtained from FDTD Simulation. The averaged SAR over weight is represented in blue; the averaged SAR over volume is represented in red.*

4. Discussion

The value of the smartwatch radiation changes depending on the body part considered: the structure of different human tissues, in fact, reacts differently.

As can be seen in *Table 6* and in *Figure 17*, the averaged SAR over 1 g has higher peak values than the averaged SAR over 10 g. In addition, the averaged SAR over volume is lower than the averaged SAR over weight.

The values of SAR [W/kg] obtained thanks to FDTD simulations are plausible, and so lower than the limits imposed by the regulations in force. In fact, smartwatches generally have very low SAR values, like many other devices without a SIM card. Therefore, despite smartwatches are wearable devices, they cannot be considered harmful to the user's health. Furthermore, the smartwatch is held on the wrist, which is a part of the body for which radiation is potentially much less dangerous than in other parts of the body, like the head. For this reason, in fact, the limit of SAR for wearables devices is generally set to 4.0 W/kg if we refer this measure to limbs [33].

Unfortunately, we cannot consider these SAR values as universal values, because each person could have a different sensitivity to radiation exposure, not only based on anatomy but also on the position and type of use of the device.

5. Concluding Remarks

Recently, the market for smart wearable devices such as smartwatches and smart-bracelets, has been rapidly growing, which generates significant industrial and public interest in the technology [5]. Although these technically advanced devices have proved to be of immense benefit – both from the point of view of smart communication and from the point of view of monitoring the daily activities of an individual – their rapid development and continuous improvement have had the unintended consequence of creating a knowledge gap in the study of interactions between the device and human tissues [14]. In fact, wearable and implantable devices require the transmitting and receiving of electromagnetic waves near and through the body, which at high enough exposure levels may damage proximate tissues. The main aspect is that they are in direct contact with the human skin so the determination of potential health effects is still an open issue [17].

While much has been done on the computation of the specific absorption rate (SAR) and standardization of mobile phones, other wearable devices deserve further attention [14]. In addition, the studies that have been performed until now only considered tissue composition for the head and torso structures and did not consider an anatomical human-body model shape and dimension.

Therefore, in order to fill in the aforementioned gap in research, the purpose of this study was the electromagnetic characterization of the wrist, useful for the determination, through FDTD simulations, of the effects of the electromagnetic fields generated by smartwatches Bluetooth antennas on the human tissues.

The homemade FDTD code developed for the electric field computation on the anatomical wrist-model revealed to be suitable in presence of a smartwatch as source. The values of SAR [W/kg] investigated in layered biological structures are plausible, and so lower than the limits imposed by the regulations in force. Unfortunately, we cannot consider these SAR values as universal values, because each person could have a different sensitivity to radiation exposure.

6. Future Perspective

The purpose of this study was the electromagnetic characterization of the wrist, useful for the determination, through FDTD simulations, of the effects of the electromagnetic fields generated by Bluetooth antennas on the human tissues.

The study of the interaction between a smartwatch and the individual's tissues has been carried out only through FDTD simulations that allow predicting electric field strength and SAR values. An additional and more detailed study of the device – human tissues interaction could also be implemented through measurements in a reverberation chamber.

Reverberation chambers (RC) are electrically large cavities where the electromagnetic field is statistically uniform, isotropic and randomly polarized [45]. A lot of effort has been devoted in develop theoretical models able to accurately describe the chamber field properties; on the other hand, also a lot of numerical modelling has been developed to account for actual device presence in RC [46]. The reverberation chamber is also widely used for shielding effectiveness measurements, for Wi-Fi communication system testing and for antenna testing thanks to the capability of create real environment propagation characteristics [46]. The peculiarity of the RC to generate a wave with statistically random incidence, in fact, has developed applications in the field of human exposure assessment to electromagnetic field to reproduce real exposure conditions [46].

In this study, we were unable to perform the simulation in the reverberation chamber, due to the stringent regulations on COVID-19. In fact, due to the way the RC is built, it does not allow the recirculation of the air, necessary to carry out the measurements in total safety. Thus, future studies may contemplate the use of the reverberation chamber in order to confirm the electric field strength and SAR values predicted thanks to the FDTD simulation.

References

[1] H.H. Hsu, C.Y. Chang & C.H. Hsu; "Big Data Analytics for Sensor-Network Collected Intelligence". *Morgan Kaufmann*; 2017.

[2] S. Ahmadi; "5G NR: Architecture, Technology, Implementation, and Operation of 3GPP New Radio Standards". *Academic Press*; 2019.

[3] P. Dominique & P. Crégo; "Wearables, Smart Textiles & Smart Apparel". *Elsevier*; 2018.

[4] A. Bohr, S. Colombo & H. Jensen; "Future of Microfluidics in Research and in the Market". *Microfluidics for Pharmaceutical Applications*; 425-465. *William Andrew Publishing*; 2019.

[5] X. Tao; "Wearable electronics and photonics". *Elsevier*; 2005.

[6] C. Perera, C.H. Liu & S. Jayawardena, "The emerging internet of things marketplace from an industrial perspective: A survey". *IEEE Transactions on Emerging Topics in Computing*; 3(4), 585-598. 2015.

[7] B. Nascimento, T. Oliveira & C. Tam; "Wearable technology: What explains continuance intention in smartwatches?". *Journal of Retailing and Consumer Services*; 43, 157-169. 2018.

[8] J. Choi & S. Kim; "Is the smartwatch an IT product or a fashion product? A study on factors affecting the intention to use smartwatches". *Computers in Human Behavior*; 63, 777-786. 2016.

[9] M.E. Cecchinato, A.L. Cox & J. Bird; "Smartwatches: the Good, the Bad and the Ugly?". *Proceedings of the 33rd Annual ACM Conference extended abstracts on human factors in computing systems*; 2133-2138. 2015.

[10] B. Reeder & A. David; "Health at hand: a systematic review of smart watch uses for health and wellness". *Journal of biomedical informatics*; 63, 269-276. 2016.

[11] N. Anggraini, E.R. Kaburuan, G. Wang & R. Jayadi; "Usability Study and Users' Perception of Smartwatch: Study on Indonesian Customer". *Procedia Computer Science*; 161, 1266-1274. 2019.

[12] L. Ryzhyk; "The ARM Architecture". *Chicago University, Illinois, EUA*; 2006.

[13] H.W. Chen, J.H. Lee, B.Y. Lin, S. Chen & S.T. Wu; "Liquid crystal display and organic light-emitting diode display: present status and future perspectives". *Light: Science & Applications*; 7(3), 17168-17168. 2018.

[14] A. Gravina, F. Moglie, L. Bastianelli & V.M. Primiani; "Flexible FDTD Simulation for the Wireless Earphone Exposure Evaluation". *2020 International Symposium on Electromagnetic Compatibility-EMC EUROPE*; 1-6. *IEEE*; 2020.

[15] M.G. Stabin; "Radiation Dosimetry: Formulations, Models, and Measurements". *Basic Sciences of Nuclear Medicine*; 129-144. *Springer, Berlin, Heidelberg*; 2010.

[16] S.E. Hong, A.K. Lee, J.H. Kwon & J.K. Pack; "Numerical compliance testing of human exposure to electromagnetic radiation from smart-watches". *Physics in Medicine & Biology*; 61(19), 6975. 2016.

[17] World Health Organization; "Radiation, Environmental Health, & World Health Organization". *Establishing a dialogue on risks from electromagnetic fields*; 2002.

[18] I. Poole, I; "Wi-Fi/WLAN Channels, Frequencies, Bands & Bandwidths". *Radio-Electronics. Saatavissa: http://www.radioelectronics.com/info/wireless/wi-fi/80211-channels-number-frequenciesbandwidth*. Php; 27. 2016.

[19] T.E. Bogale, X. Wang & L.B. Le; "mmWave communication enabling techniques for 5G wireless systems: A link level perspective". *MmWave Massive MIMO*; 195-225. *Academic Press*; 2017.

[20] T. Pattnayak, G. Thanikachalam & A.P. Family; "Antenna design and RF layout guidelines". *Cypress Semiconductor: San Jose, CA, USA*; 17. 2015.

[21] K. Zhao, Z. Ying & S. He; "Antenna designs of smart watch for cellular communications by using metal belt". 9th *European Conference on Antennas and Propagation, EuCAP*; 1-5. *IEEE*; 2015.

[22] S.W. Su & Y.T. Hsieh; "Integrated metal-frame antenna for smartwatch wearable device". *IEEE Transactions on Antennas and Propagation*; 63(7), 3301-3305. 2015.

[23] A. Waug & A. Grant; "Ross & Wilson Anatomy and physiology in health and illness E-book". *Elsevier Health Sciences*; 2014.

[24] P.K. Levangie & C.C. Norkine; "Joint structure and function: A comprehensive analysis". *Philadelphia: The F.A. Davis Company*; 2005.

[25] C.T. Wadsworth; "Wrist and hand examination and interpretation". *Journal of Orthopaedic & Sports Physical Therapy*; 5(3), 108-120. 1983.

[26] D.A. Neumann; "Kinesiology of the musculoskeletal system-e-book: foundations for rehabilitation". *Elsevier Health Sciences*; 2013.

[27] I.G. Zubal, C.R. Harrell, E.O. Smith, A.L. Smith & P. Krischlunas; "Two dedicated software, voxel-based, anthropomorphic (torso and head) phantoms". *Proceeding of the International Conference at the National Radiological Protection Board*; 105-111. 1995.

[28] W.S. Snyder, M.R. Ford, G.G. Warner & H.L. Fisher; "Estimates of absorbed fractions for monoenergetic photon source uniformly distributed in various organs of a heterogeneous phantom". *Medical Internal Radiation Dose Committee (MIRD)*; 5(3). *New York: Society of Nuclear Medicine*; 1978.

[29] X.G. Xu, T.C. Chao & A. Bozkurt; "VIP-Man: an image-based whole-body adult male model constructed from color photographs of the Visible Human Project for multi-particle Monte Carlo calculations". *Health Physics*; 78(5), 476-486. 2000.

[30] H. Zaidi & X.G. Xu; "Computational anthropomorphic models of the human anatomy: the path to realistic Monte Carlo modeling in radiological sciences". *Annu. Rev. Biomed. Eng.*; 9, 471-500. 2007.

[31] I.G. Zubal, C.R. Harrell, E.O. Smith, Z. Rattner, G. Gindi & P.B. Hoffer; "Computerized three-dimensional segmented human anatomy". *Medical physics*; 21(2), 299-302. 1994.

[32] J.B. Schneider; "Understanding the finite-difference time-domain method". S*chool of electrical engineering and computer science Washington State University*; 28. 2010.

[32] A. Taflove & S.C. Hagness; "Computational electrodynamics: the finite-difference time-domain method". *Artech house*; 2005.

[33] J. Jin; "Electromagnetic analysis and design in magnetic resonance imaging". *CRC press*; 1998.

[34] D. Poljak & M. Cvetkovic; "Human Interaction with Electromagnetic Fields: Computational Models in Dosimetry". *Academic Press*; 2019.

[35] K. Guido & A. Kiourti; “Wireless Wearables and Implants: A Dosimetry Review”. *Bioelectromagnetics*; 41(1), 3-20. 2020.

[36] D.A. Sánchez-Hernández; “High frequency electromagnetic dosimetry”. *Artech House*; 2009.

[37] P. Stavroulakis; “Biological effects of electromagnetic fields: Mechanisms, modeling, biological effects, therapeutic effects, international standards, exposure criteria”. *Springer Science & Business Media*; 2013.

[38] J.D. Bronzino; “Biomedical Engineering Handbook 2”. *Springer Science & Business Media*; 2000.

[39] S. Grimnes & O.G. Martinsen; “Bioimpedance and Bioelectricity Basics”. *Elsevier*; 2015.

[40] H.P. Schwan; "Electrical properties of tissue and cell suspensions". Advances in biological and medical physics; 5, 147-209. Elsevier; 1957.

[41] K. Górska, A. Horzela & A. Lattanzi; “Composition law for the Cole-Cole relaxation and ensuing evolution equations”. *Physics Letters A*; 383(15), 1716-1721. 2019.

[42] J.M. Bumgarner, C.T. Lambert, A.A. Hussein, D.J. Cantillon, B. Baranowski, K. Wolski & K.G. Tarakji; “Smartwatch algorithm for automated detection of atrial fibrillation”. *Journal of the American College of Cardiology*; 71(21), 2381-2388. 2018.

[43] J. Wasserlauf, C. You, R. Patel, A. Valys, D. Albert & R. Passman; “Smartwatch performance for the detection and quantification of atrial fibrillation”. *Circulation: Arrhythmia and Electrophysiology*; 12(6). 2019.

[44] T.M. Manini, T. Mendoza, M. Battula, A. Davoudi, M. Kheirkhahan, M.E. Young & P. Rashidi; “Perception of older adults toward smartwatch technology for assessing pain and related patient-reported outcomes: pilot study”. *JMIR mHealth and uHealth*; 7(3). 2019.

[45] D.A. Hill; “Electronic mode stirring for reverberating chambers”. *IEEE Transactions on Electromagnetic Compatibility*; 36, 294–299. 1994.

[46] F. Moglie & V.M. Primiani; “Efficient Measurement of Radiated Emission in Reverberation Chamber”. *Machine Copy for Proofreading*; 2012.